metals

MDPI

Article

Zn and P Alloying Effect in Sub-Rapidly Solidified $LaFe_{11.6}Si_{1.4}$ Magnetocaloric Plates

Pingxia Jin [1,2], Yuqiang Li [1,2], Yuting Dai [1,2], Zhishuai Xu [1,2], Changjiang Song [1,2], Zhiping Luo [3], Qijie Zhai [1,2], Ke Han [4] and Hongxing Zheng [1,2,*]

1 School of Materials Science and Engineering, Shanghai University, Shanghai 200444, China; m13591488311_1@163.com (P.J.); li18621096301@163.com (Y.L.); dytbbd@126.com (Y.D.); xzsshu@shu.edu.cn (Z.X.); riversxiao@shu.edu.cn (C.S.); qjzhai@shu.edu.cn (Q.Z.)
2 Center for Advanced Solidification Technology, Shanghai University, Shanghai 200444, China
3 Department of Chemistry and Physics, Fayetteville State University, Fayetteville, NC 28301, USA; zhipingluo@gmail.com
4 National High Magnetic Field Laboratory, Florida State University, Tallahassee, FL 32310, USA; han@magnet.fsu.edu
* Correspondence: hxzheng@shu.edu.cn; Tel.: +86-21-6613-6563

Received: 28 March 2019; Accepted: 10 April 2019; Published: 11 April 2019

Abstract: The occupation mechanism and magnetic transition behavior of trace Zn and P alloying in the sub-rapidly solidified $LaFe_{11.6}Si_{1.4}$ magnetocaloric plates were investigated. The $LaFe_{11.6}Si_{1.4}$, $LaFe_{11.6}Si_{1.4}Zn_{0.03}$, and $LaFe_{11.6}Si_{1.4}P_{0.03}$ plates were fabricated using the centrifugal casting method in the present work. Experimental results showed that both Zn and P elements were distributed in the La_5Si_3 and LaFeSi phases during sub-rapid solidification. After annealed at 1373 K for 72 h, the $LaFe_{11.6}Si_{1.4}$ plate underwent a second-order magnetic transition, while both the $LaFe_{11.6}Si_{1.4}Zn_{0.03}$ and $LaFe_{11.6}Si_{1.4}P_{0.03}$ plates underwent a first-order transition. In combination with X-ray diffraction results, it was proposed that both Zn and P atoms prefer to enter the 96*i* site substituting for FeII/Si atoms according to the density-functional reconstruction of crystallographic structure. The Zn addition led to a slight decrease in magnetic entropy change from 7.0 to 5.9 J/(kg·K), while the P addition strikingly enhanced this property to 31.4 J/(kg·K) under a magnetic field change of 3 T. The effective refrigeration capacity of the annealed $LaFe_{11.6}Si_{1.4}P_{0.03}$ plate reached 189.9 J/kg.

Keywords: La–Fe–Si magnetocaloric materials; magnetic transition; density-functional theory; magnetic entropy; centrifugal casting

1. Introduction

Solid-state magnetic refrigeration has been considered to be a highly competitive alternative to the conventional vapor-compression technology based on the magnetocaloric effect [1]. As early as 1976, Brown discovered that the heavy rare-earth Gd demonstrated a magnetic entropy change as high as 13.17 J/(kg·K) under a magnetic field change of 7 T in the vicinity of 293 K [2]. Since then, heavy rare-earth Gd has been taken as an important benchmark for the research and development of room-temperature magnetocaloric materials [3,4]. During the past two decades, a few promising candidates, including $Gd_5Si_2Ge_2$ [5–7], $MnFeP_{1-x}As_x$(Si) [8,9], Heusler Ni_2MnX (X = Ga, Sn, In) [10–12], $La(Fe,Si)_{13}$ [13,14], $LaMnO_3$ magnetite [15,16], and R_2Fe_{17} system [17,18], were found, among which $La(Fe,Si)_{13}$ attracted significant attention due to the advantages afforded by its non-toxic constituent elements, giant magnetocaloric effect, small thermal/magnetic hysteresis, and high thermal conductivity [19].

A lot of effort has been spent on the synthesis of $La(Fe,Si)_{13}$. The main advantage of powder metallurgy [20–22] lies in its flexible gradient compositional control, which is beneficial for broadening

the refrigeration temperature window; however, high-temperature annealing is still needed for the diffusion-controlled formation of the La(Fe,Si)$_{13}$ (τ_1) phase [23]. Although melt spinning could directly produce a high proportion of τ_1 phase during rapid solidification, and the resultant refined grains greatly shorten the post-annealing procedure, it was hard to achieve practical application due to its flake-like shape [24,25]. Researchers have tried to integrate brittle La(Fe,Si)$_{13}$ particles into a continuous matrix (epoxy resin [26,27] or molten Sn [28,29], SnBi [30]) or cladded them with a thin seamless austenitic steel jacket through the powder-in-tube (PIT) technology [31]. Unfortunately, more unexpected problems arose, such as slimsy interface bonding, low thermal conductivity, and dramatic decay of magnetocaloric capacity. The only exception is that Wang et al. [32] observed excellent magnetocaloric effect with durable service life in the La(Fe,Si)$_{13}$H$_y$/In composite where they hot pressed La(Fe,Si)$_{13}$H$_y$ particles with solid-state indium powder at 413 K (lower than the melting point 430 K of indium element). Additionally, the centrifugal casting method [33] was also employed to produce a sub-rapidly solidified La(Fe,Si)$_{13}$ thin plate.

On the other hand, fourth elemental alloying has been extensively attempted to adjust the magnetic transition, including C [34], H [35], Co [36], Ni [37], Cu [38], Nd [39], Ce [40], etc. For instance, Anh et al. [41] reported that the characteristic temperature of magnetic transition in the LaFe$_{11.44}$Si$_{1.56}$ alloy linearly increased with Nd partially replacing La, and was accompanied by volume shrinkage of the unit-cell. However, the occupation mechanism for the fourth elements in La(Fe,Si)$_{13}$ remains unclear, and even controversial. Rosca et al. [42] proposed H atoms preferred the 48*f* interstitial site (a FeII/Si-based asymmetric pyramid with one La vertex [43]) in LaFe$_{11.31}$Si$_{1.69}$H$_{1.45}$ based on neutron diffraction results, while Bao et al. [44] suggested the 24*d* interstitial site (an octahedral site with four FeII/Si and two La nearest neighbors [45]) based on the fact that all Fe–Fe bonds become longer, and the shortest inter-cluster bond (B4) changes the most [46]. One more example is that Phejar et al. [47] concluded that C atoms entered the 48*f* interstitial site, which differs from the viewpoint of Hai et al. [43] who argue in favor of the 24*d* interstitial site. Our recent work [48] supported the 24*d* interstitial site for C alloying in LaFe$_{11.6}$Si$_{1.4}$ according to the crystallographic structure reconstruction based on density-functional theory (DFT) [49–51], and it was proven that density-functional reconstruction is an effective tool to explain the magnetic transition behavior by quantitatively measuring the length change of Fe–Fe bonds. Save for these limited studies on light elements, it was simply taken for granted that rare-earth elements (Nd [52], Ce [53,54], and Pr [55]) substitute for La and transition-metals (Co [56,57], Mn [58–60], Ni [61], and Cu [38]) for Fe when alloying La(Fe,Si)$_{13}$, although no supporting evidence was provided. Against this background, trace Zn (metallic element) and P (non-metallic element) alloying was studied in a sub-rapidly solidified La(Fe,Si)$_{13}$ plate in the present work, with an emphasis on the magnetic transition behavior and occupation mechanism.

2. Experimental

Three button ingots with a weight of about 120 g and nominal compositions of LaFe$_{11.6}$Si$_{1.4}$, LaFe$_{11.6}$Si$_{1.4}$Zn$_{0.03}$, and LaFe$_{11.6}$Si$_{1.4}$P$_{0.03}$ (at.%) were prepared using levitation melting from commercial pure La (99.9 wt.%), Fe (99.99 wt.%), Si (99.999 wt.%), and Zn (99.8 wt.%). All ingots were remelted four times to ensure homogeneity. The obtained ingots were then spun into plates with a dimension of ~60 × 40 × 2.5 mm^3 using a centrifugal casting setup in argon under a cooling rate of ~5000 K/s. Experimental details have been described elsewhere [62]. Half of the plates were sealed in quartz tubes and annealed at 1373 K for 72 h, followed by water quenching.

Microstructure and elemental analyses were performed using an electron probe microanalyzer (EPMA-8050G, Shimadzu, Tokyo, Japan) equipped with a wavelength-dispersive spectrometer (WDS). Differential scanning calorimetric measurements (DSC, Netzsch 404 F3, NETZSCH-Gerätebau GmbH, Selb, Germany) were carried out to clarify high-temperature phase transition behavior at a heating/cooling rate of 20 K/min. X-ray diffraction (XRD, Dlmax-2500, Rigaku, Osaka, Japan) with Cu K_α radiation was conducted to detect the phase and crystal structure. Magnetic

properties were measured using a physical property measurement system (PPMS-9, Quantum Design, San Diego, CA, USA).

3. Results and Discussion

3.1. Phase and Microstructure

A typical honeycomb-like refined microstructure of the sub-rapidly solidified $LaFe_{11.6}Si_{1.4}$ plate is shown in Figure 1a, which is different from the coarse dendrites usually obtained in conventional arc-melted alloy [63]. WDS analyses reveal that the black, grey, and white areas represent α(Fe), LaFeSi, and La_5Si_3 phases, respectively, as marked by red arrows in Figure 1b. Similar SEM images of the $LaFe_{11.6}Si_{1.4}Zn_{0.03}$ and $LaFe_{11.6}Si_{1.4}P_{0.03}$ plates were not shown for clarity. Both Zn/P elements were distributed in the LaFeSi and La_5Si_3 phases, and no Zn/P element was detected in the α(Fe) phase. The elemental mappings of La, Fe, Si, and Zn in the sub-rapidly solidified $LaFe_{11.6}Si_{1.4}Zn_{0.03}$ plate are shown in Figure 1c (similar elemental mappings of $LaFe_{11.6}Si_{1.4}P_{0.03}$ are not shown here).

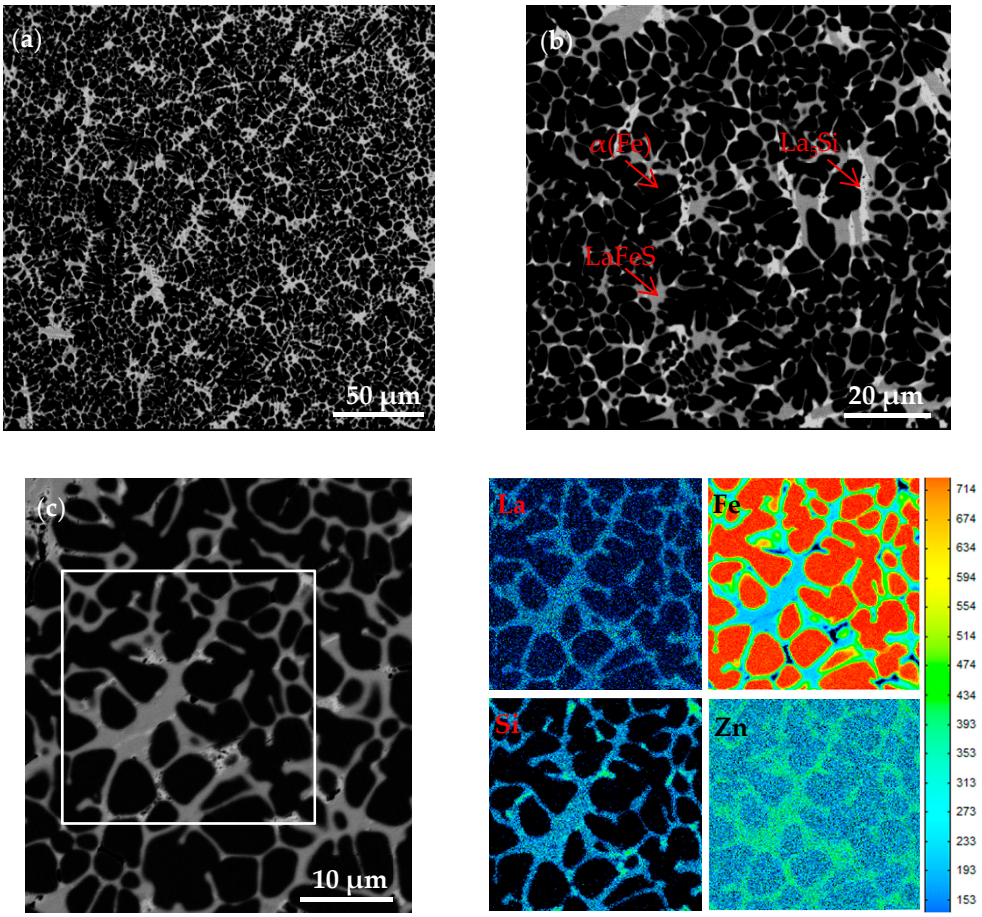

Figure 1. Backscatter SEM image of the sub-rapidly solidified $LaFe_{11.6}Si_{1.4}$ plate (**a**) and an enlarged image showing the α(Fe), LaFeSi, and La_5Si_3 phases (**b**). (**c**) Backscatter SEM image of $LaFe_{11.6}Si_{1.4}Zn_{0.03}$ plate and the corresponding La, Fe, Si, and Zn elemental distribution within the area marked by a square in Figure 1c.

DSC measurements for the sub-rapidly solidified plates were used to analyze their high-temperature phase transition behavior. Here, using $LaFe_{11.6}Si_{1.4}$ as an example, a magnetic transition of the α(Fe) phase happens around 1018 K upon heating, and reverse transition occurs at 991 K upon cooling (marked by circles in Figure 2). According to previous investigation [64], solid LaFeSi, τ_1, and α(Fe) phases melt at 1394, 1558, and 1682 K, respectively, upon heating. The primary α(Fe) phase

first forms at 1682 K upon cooling, and then τ_1 phase through a α(Fe) + $L_{La} \rightarrow \tau_1$ peritectic reaction [65]. With Zn/P alloying, there is almost no difference for the high-temperature transition behaviors (not shown here). The formation τ_1 phase in all three sub-rapidly solidified plates annealed at 1373 K is fully completed through peritectoid interdiffusion between the α(Fe) and LaFeSi phases [62]. A few weak exothermic peaks close to 1464 K correspond to the formation of La_5Si_3 phase from residual liquid τ_1 phase, which can be easily confirmed by the shrinkage cavities. All annealed plates consist of τ_1 matrix phase and a small amount of black α(Fe) phase, with a few white areas indicating LaFeSi phase visible in the $LaFe_{11.6}Si_{1.4}P_{0.03}$ plate (Figure 3a,c). One can observe that both Zn and P elements homogeneously dissolved into the τ_1 matrix according to the WDS analyses (Figure 3b,d).

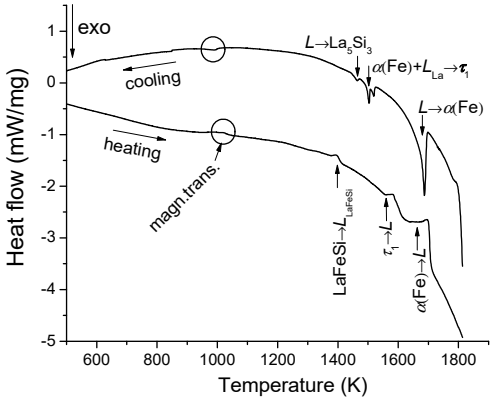

Figure 2. High-temperature differential scanning calorimetry (DSC) chart of the sub-rapidly solidified $LaFe_{11.6}Si_{1.4}$ plate with a heating/cooling rate of 20 K/min.

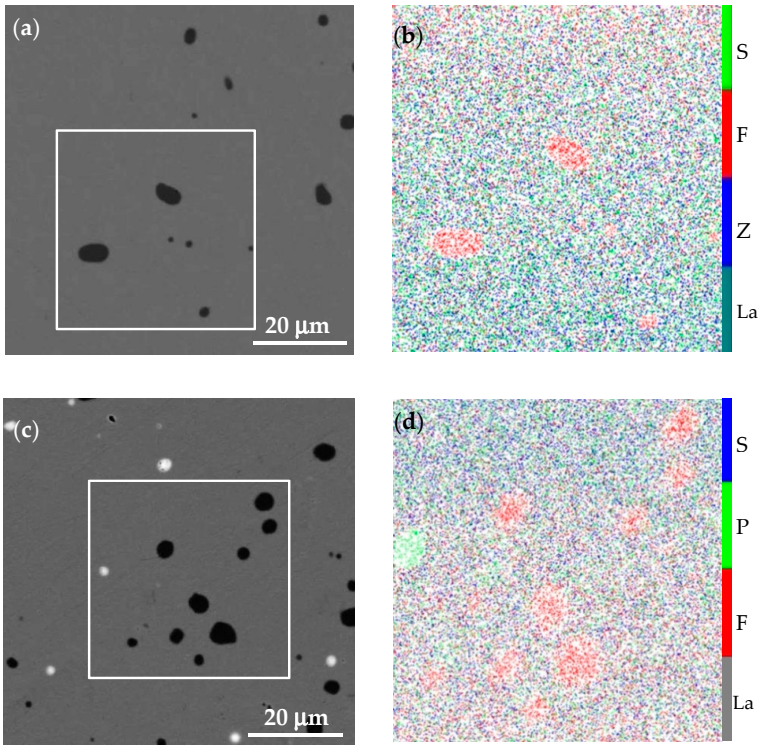

Figure 3. Backscatter SEM images of the annealed $LaFe_{11.6}Si_{1.4}Zn_{0.03}$ (**a**) and $LaFe_{11.6}Si_{1.4}P_{0.03}$ plates (**c**). Images (**b**) and (**d**) are the corresponding elemental distributions within the areas marked by squares in (**a**) and (**c**), respectively.

X-ray diffraction peaks shown in Figure 4a are well indexed to be τ_1 and α(Fe) phases [66]. The main diffraction peak at 44.7° from τ_1 phase for both Zn/P-alloyed plates shifts towards higher angle regime in contrast to that of $LaFe_{11.6}Si_{1.4}$, as shown in Figure 4b (enlarged image), which implies that the unit-cell shrank with Zn/P alloying. Using the least square method, the lattice parameters of the τ_1 phase for the annealed $LaFe_{11.6}Si_{1.4}$, $LaFe_{11.6}Si_{1.4}Zn_{0.03}$, and $LaFe_{11.6}Si_{1.4}P_{0.03}$ plates are calculated to be 1.1473 ± 0.006, 1.1468 ± 0.0059, and 1.1471 ± 0.0052 nm, respectively.

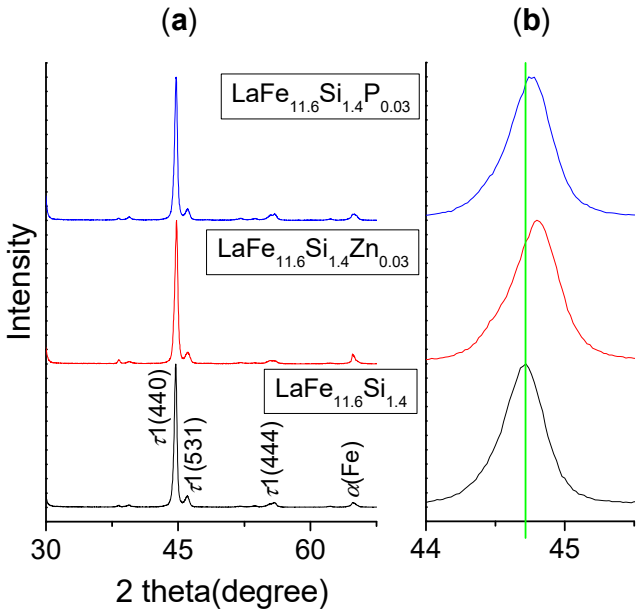

Figure 4. X-ray diffraction (XRD) patterns of the annealed $LaFe_{11.6}Si_{1.4}$, $LaFe_{11.6}Si_{1.4}Zn_{0.03}$, and $LaFe_{11.6}Si_{1.4}P_{0.03}$ plates at room temperature (**a**), and (**b**) enlarged τ_1(440) peak showing the shift towards higher angle regime with Zn/P alloying.

3.2. Magnetic Transition and Magnetocaloric Effect

Magnetization curves as a function of temperature (*M*-*T*) were measured under a low magnetic field of 0.05 T (Figure 5a–c). The Curie temperature of $LaFe_{11.6}Si_{1.4}$, $LaFe_{11.6}Si_{1.4}Zn_{0.03}$, and $LaFe_{11.6}Si_{1.4}P_{0.03}$ were determined to be 205, 192, and 194 K, respectively, from the d*M*/d*T* curves upon heating (Figure 5d–f). All the annealed plates show a drop of magnetization intensity upon heating, which corresponds to a ferromagnetic-paramagnetic transition, and reverse transition upon cooling [67]. The characteristic transition temperature decreased by 13 and 11 K, respectively, with Zn and P alloying compared to that of $LaFe_{11.6}Si_{1.4}$. This agrees to the principle that the Curie temperature always increases with expansion of the unit-cell and decreases with shrinkage in $La(Fe,Si)_{13}$ [68], although some unknown factors cannot be excluded. We will discuss the occupation mechanism in Section 3.3. It should be noted that the *M*(*T*) curve of $LaFe_{11.6}Si_{1.4}P_{0.03}$ is different for both $LaFe_{11.6}Si_{1.4}$ and $LaFe_{11.6}Si_{1.4}Zn_{0.03}$. A clear slope change for $LaFe_{11.6}Si_{1.4}$ and $LaFe_{11.6}Si_{1.4}Zn_{0.03}$ can be observed, in contrast to the sharp decrease in $LaFe_{11.6}Si_{1.4}P_{0.03}$, and the nonzero remnant magnetization above the Curie temperature is associated with the residual α(Fe) phase [69].

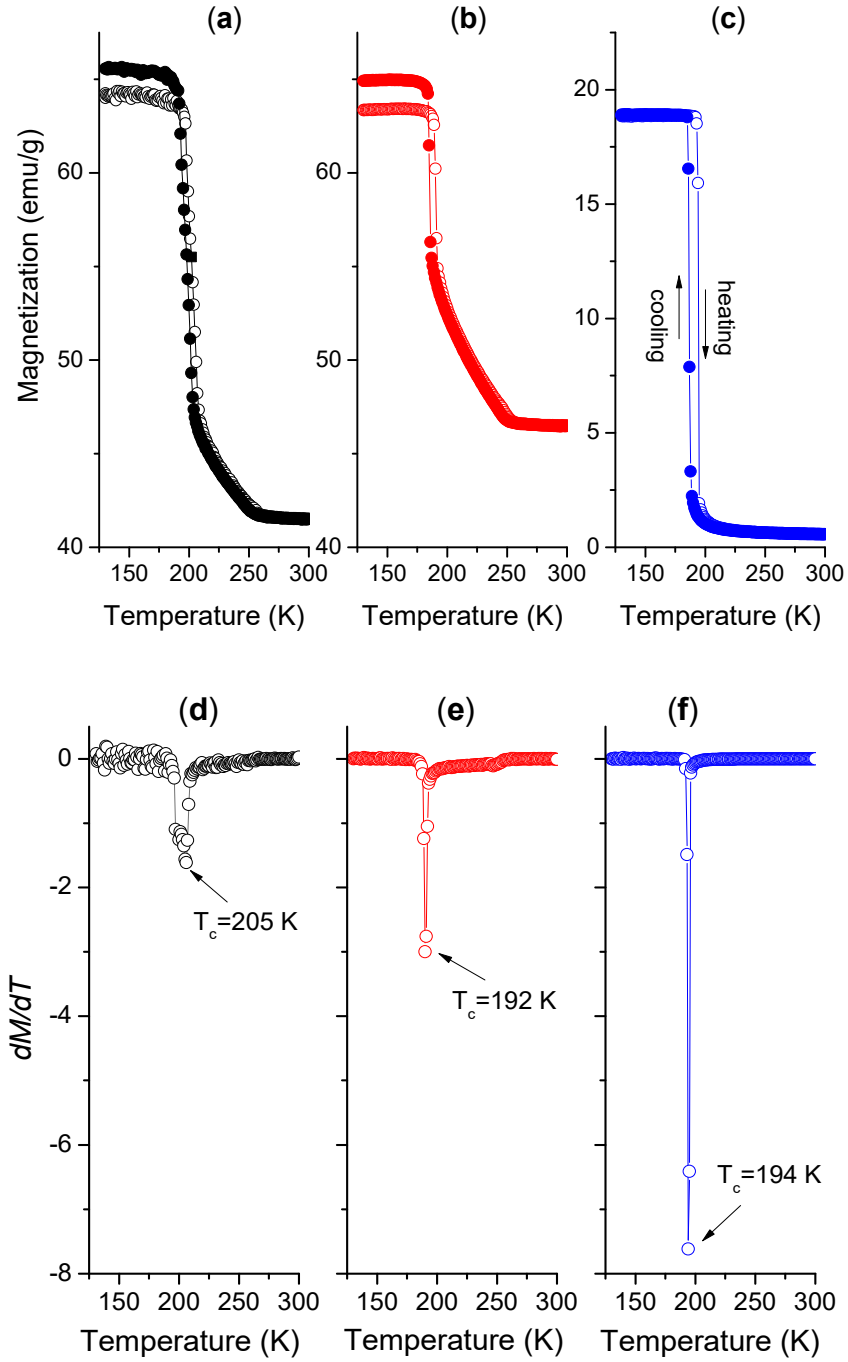

Figure 5. Magnetization curves measured under a low magnetic field of 0.05 T for annealed $LaFe_{11.6}Si_{1.4}$ (**a**), $LaFe_{11.6}Si_{1.4}Zn_{0.03}$ (**b**), and $LaFe_{11.6}Si_{1.4}P_{0.03}$ (**c**), respectively. Plots (**d**–**f**) are the corresponding d*M*/d*T* curves upon heating.

Several selected isothermal magnetization curves (*M*-*H*) around the magnetic transition (near the Curie temperature) under a magnetic field change of 3 T were measured at an interval of 3 K (Figure 6a–c). One can observe that the magnetization curves for the $LaFe_{11.6}Si_{1.4}$ plate have characteristics of a second-order transition, while both the $LaFe_{11.6}Si_{1.4}Zn_{0.03}$ and $LaFe_{11.6}Si_{1.4}P_{0.03}$ plates show S-shaped magnetization curves, which are a typical feature for the first-order itinerant electro-metamagnetism [70]. The magnetic hysteresis effects (shadowed areas marked in Figure 6b,c) also confirm the first-order nature of the magnetic transition, and the $LaFe_{11.6}Si_{1.4}$ plate underwent a second-order transition without any hysteresis (Figure 6a). Additionally, it was also well accepted

that the type of phase transition can be judged using the Arrott plots (Figure 6d–f) [71,72] according to the Inoue-Shimizu model [73]. The free energy of a magnetic system is expressed by the Landau expansion in powers of magnetization in this model. The type of phase transition is closely related to the sign of the Landau coefficient at the Curie temperature, which can be obtained from the Arrott plots. If there are "S-bend" Arrott curves near the Curie temperature, the Landau coefficient is negative and the transition is first order; otherwise, it is positive, and the transition is second order. As seen in Figure 6d–f, a second-order transition happened in the $LaFe_{11.6}Si_{1.4}$ plate with regard to an almost linear behavior in the Arrott plots, while the magnetic transition in both the $LaFe_{11.6}Si_{1.4}Zn_{0.03}$ and $LaFe_{11.6}Si_{1.4}P_{0.03}$ plates changed from the second order to the first order according to the characteristic "S-bend" Arrott plots.

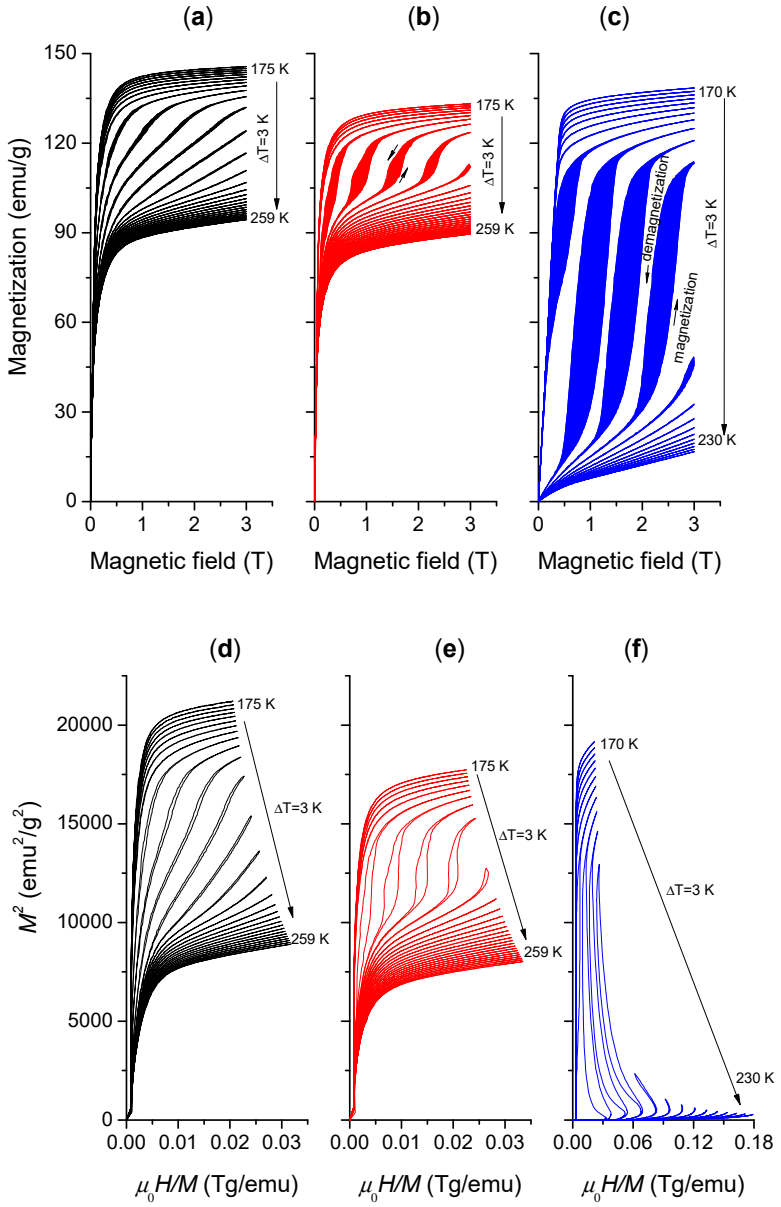

Figure 6. Isothermal magnetization curves for the annealed $LaFe_{11.6}Si_{1.4}$ (**a**), $LaFe_{11.6}Si_{1.4}Zn_{0.03}$ (**b**), and $LaFe_{11.6}Si_{1.4}P_{0.03}$ (**c**), respectively. Shadowed areas indicate the magnetic hysteresis. Images (**d**–**f**) are the corresponding Arrott plots.

The magnetic entropy change (ΔS_M) can be estimated using the classical Maxwell Equation $\Delta S_M(T,H) = \mu_0 \int_0^H \left(\frac{\partial M}{\partial T}\right)_H dH$ [50], as shown in Figure 7a–c. The second-order transition occurred with Zn alloying in $LaFe_{11.6}Si_{1.4}$, and as a result, the maximum $|\Delta S_M|$ value decreased from 7.0 to 5.9 J/(kg·K) under a magnetic field change of 3 T. P alloying led to a complete first-order magnetic transition, and thus, the maximum $|\Delta S_M|$ value reached to 31.4 J/(kg·K), which is higher than those of the $LaFe_{11.6}Si_{1.4}$ plate (22.2 J/(kg·K) annealed at 1373 K for 3 h [62]) and the suction-cast rod (27.8 J/(kg·K) annealed at 1373 K for 100 h [48]). Additionally, refrigeration capacity (RC) was taken as another important indicator to assess magnetocaloric effect. RC represents the amount of heat that can be transferred between the cold sink and the hot sink within one thermodynamic cycle, which systematically takes into account both peak values and temperature intervals of ΔS_M, and is defined as $RC = \int_{T_{cold}}^{T_{hot}} |\Delta S_M(T)| dT$ [16,18], where T_{hot} and T_{cold} are the corresponding temperatures at full width half the maximum peak value of ΔS_M (as shown by stripped area in Figure 7a). After subtracting average hysteresis losses, the effective RC_{eff} values for the annealed $LaFe_{11.6}Si_{1.4}$, $LaFe_{11.6}Si_{1.4}Zn_{0.03}$, and $LaFe_{11.6}Si_{1.4}P_{0.03}$ are 89.3, 72.7, and 189.9 J/kg, respectively.

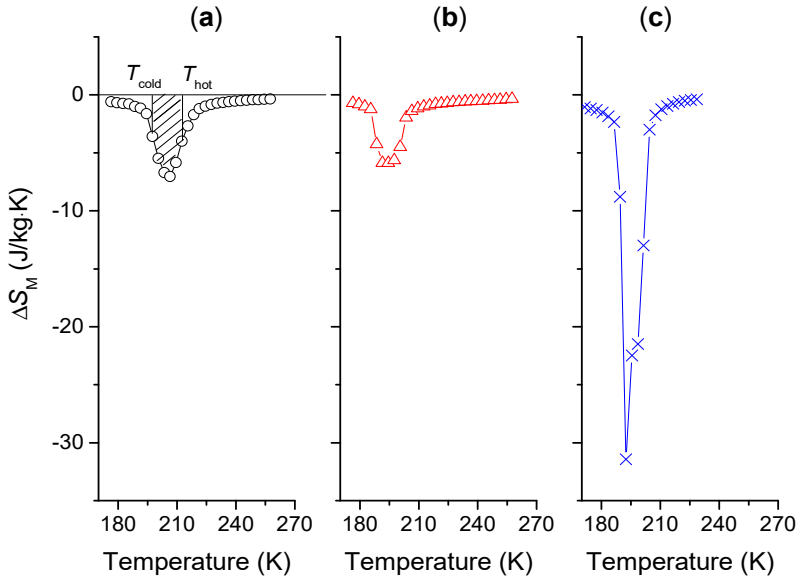

Figure 7. Calculated magnetic entropy changes (ΔS_M) under a magnetic field change of 3 T for the annealed $LaFe_{11.6}Si_{1.4}$ (**a**), $LaFe_{11.6}Si_{1.4}Zn_{0.03}$ (**b**), and $LaFe_{11.6}Si_{1.4}P_{0.03}$ (**c**), respectively. Striped area in (a) was taken as an example to indicate the refrigeration capacity.

3.3. Occupation Mechanism

DFT was introduced to reconstruct the crystallographic structure of the unit-cell so as to explore the occupation mechanism of Zn/P alloying in $LaFe_{11.6}Si_{1.4}$. An ideal crystallographic unit-cell of $NaZn_{13}$-type $LaFe_{11.6}Si_{1.4}$ consists of 112 atoms, where the positions of 8*a*, 8*b*, and 96*i* are occupied by La, FeI, and FeII/Si atoms, respectively (Figure 8a). In the present work, commercial CASTEP code [74] was used based on the plane wave ultrasoft pseudopotential. The generalized gradient approximation (GGA) with the Perdew-Wang 1991 (PW91) functional [75] within the framework of density functional theory was adopted. The plane-wave cutoff energy was set to be 330 eV, and the number of *k*-points is 2 × 2 × 2. The electron configurations for La, Fe, Si, P, and Zn atoms were $5d^16s^2$, $3d^64s^2$, $3s^23p^2$, $3s^23p^3$, and $3d^{10}4s^2$, respectively. Geometric optimization of the convergence tolerances of geometry optimizations were listed as follows: (1) the total energy change within 5×10^{-6} eV per atom; (2) the maximum force smaller than 0.1 eV/nm; (3) the maximum stress of 0.02 GPa; and (4) the maximum displacement of 5×10^{-5} nm. BFGS minimizer24 was used to optimize the unit-cell, and we reconstructed the crystal structure using Materials Studio with lattice parameters $a = b = c = 1.1488$ nm.

A coefficient k = 1.133 was introduced so as to coordinate the X-ray diffraction experimental results and DFT reconstruction data. The calculated unit-cell volume and energy data with various Zn/P occupation sites are plotted in Figure 8b,c. Firstly, the atomic radii [76,77] of La, Fe, Si, Zn, and P are 0.187, 0.126, 0.111, 0.131, and 0.106 nm, respectively. It seems unreasonable that the substitution of Zn for 8*b* (FeI) or 96*i* (FeII/Si) would lead to the volume shrinkage in $LaFe_{11.6}Si_{1.4}$ since Zn atoms are larger than Fe and Si atoms. Similarly, replacing 8*b* (FeI) with P would result in a slight expansion of the unit-cell, although the P atom is smaller than the Fe atom, which indicates that besides the atomic radius, chemical bonds and electronegativity or other factors should be taken into consideration for the DFT calculation. According to X-ray diffraction experimental results (volume shrinkage), all of the other five occupation sites seem possible for Zn/P alloying except the P substitution for 8*b* (FeI) (Figure 8b). Based on the lowest energy principle, it was proposed that both Zn and P atoms prefer to enter the 96*i* (FeII/Si) substitution site (Figure 8c). We cannot fully exclude the possibility of partial Zn and P atoms occupying the 8*a* (La) or 8*b* (FeI) sites.

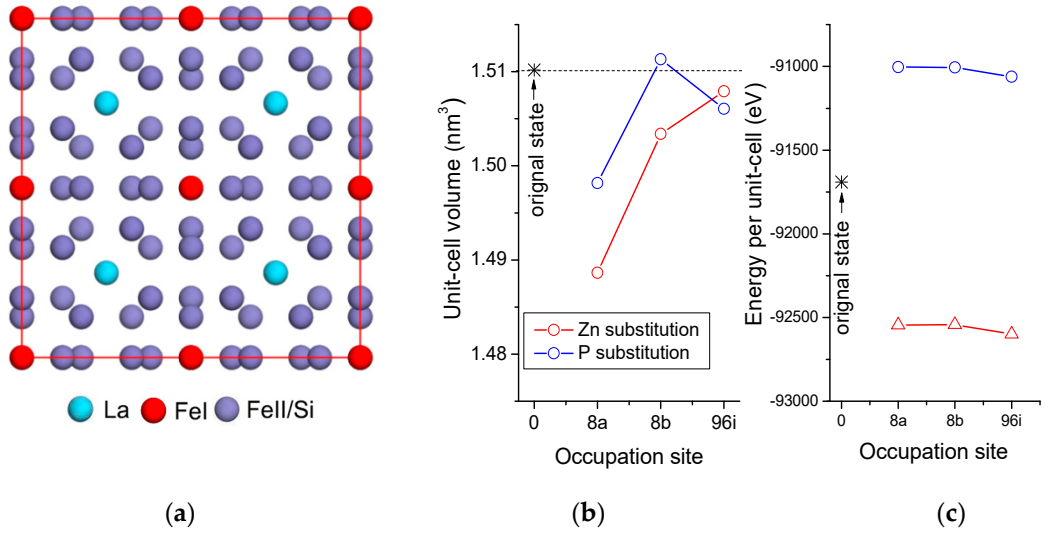

(**a**) (**b**) (**c**)

Figure 8. (010) projection of an ideal crystallographic structure of the $LaFe_{11.6}Si_{1.4}$ unit-cell (**a**), where the positions of 8*a*, 8*b*, and 96*i* are occupied by La, FeI, and FeII/Si atoms, respectively. Unit-cell volume (**b**) and energy change (**c**) for the original state of $LaFe_{11.6}Si_{1.4}$ and reconstruction with various Zn/P substitution sites.

4. Conclusions

The phase constitution, microstructure, magnetocaloric effect, and occupation mechanism of Zn/P alloyed $LaFe_{11.6}Si_{1.4}$ plates were investigated, and the following conclusions were obtained.

(1) Zn/P elements were mainly distributed in the LaFeSi and La_5Si_3 phases during centrifugal solidification. After annealing at 1373 K for 72 h, Zn/P elements were homogeneously dispersed in the τ_1 matrix and led to slight volume shrinkage of the unit-cell. Both Zn/P atoms prefer to enter the 96*i* (FeII/Si) substitution site according to the density-functional reconstruction of crystallographic structure.

(2) A second-order magnetic transition occurred in the annealed $LaFe_{11.6}Si_{1.4}$ plate, and a first-order transition in both the $LaFe_{11.6}Si_{1.4}Zn_{0.03}$ and $LaFe_{11.6}Si_{1.4}P_{0.03}$ plates. The addition of Zn/P decreased the characteristic transition temperature 11–13 K owing to lattice shrinkage.

(3) P alloying resulted in a striking increase for the maximum magnetic entropy changes from 7.0 to 31.4 J/(kg·K) under a magnetic field change of 3 T, while Zn alloying caused a slight decrease to 5.9 J/(kg·K). The effective refrigeration capacity of the annealed $LaFe_{11.6}Si_{1.4}P_{0.03}$ plate reached 189.9 J/kg.

Author Contributions: Conceptualization, H.Z.; methodology, P.J.; formal analysis, P.J., Y.D., Y.L., and Z.X.; writing—original draft preparation, P.J.; writing—review and editing, C.S., H.Z., Q.Z., Z.L., and K.H.; supervision, H.Z.

Funding: This research was funded by the National Natural Science Foundation of China (51474144) and the Shanghai Sailing Program (17YF1405900).

Acknowledgments: The authors are grateful to the National Natural Science Foundation of China and the Shanghai Sailing Program, which enabled the research to be carried out successfully.

Conflicts of Interest: The authors declare no conflict of interest.

References

1. Wang, G.F.; Zhao, Z.R.; Jing, T.; Li, Y.F.; Ma, Q.; Zhang, X.F. Enhanced magnetocaloric properties in off-stoichiometric $La_xFe_{11.5}Si_{1.5}$ alloys. *Intermetallics* **2018**, *93*, 355–359. [CrossRef]
2. Brown, G.V. Magnetic heat pumping near room temperature. *J. Appl. Phys.* **1976**, *47*, 3673–3680. [CrossRef]
3. Provenzano, V.; Shull, R.D.; Kletetschka, G.; Stutzman, P.E. $Gd_{90}Co_{2.5}Fe_{7.5}$ alloy displaying enhanced magnetocaloric properties. *J. Alloy. Compd.* **2015**, *622*, 1061–1067. [CrossRef]
4. Jayaraman, T.V.; Boone, L.; Shield, J.E. Magnetocaloric effect and refrigerant capacity in melt-spun Gd−Mn alloys. *J. Magn. Magn. Mater.* **2013**, *345*, 153–158. [CrossRef]
5. Pecharsky, A.O.; Gschneidner, K.A.; Pecharsky, V.K. The giant magnetocaloric effect between 190 and 300 K in the $Gd_5Si_xGe_{4-x}$ alloys for $1.4 \leq x \leq 2.2$. *J. Magn. Magn. Mater.* **2003**, *267*, 60–68. [CrossRef]
6. Gschneidner, K.A.; Pecharsky, V.K. Magnetic refrigeration materials. *J. Appl. Phys.* **1999**, *85*, 5365–5368. [CrossRef]
7. Aprea, C.; Greco, A.; Maiorino, A.; Masselli, C. A comparison between rare earth and transition metals working as magnetic materials in an AMR refrigerator in the room temperature range. *Appl. Therm. Eng.* **2015**, *91*, 767–777. [CrossRef]
8. Tegus, O.; Brück, E.; Buschow, K.H.J.; de Boer, F.R. Transition-metal-based magnetic refrigerants for room-temperature applications. *Nature* **2012**, *415*, 150–152. [CrossRef]
9. Yibole, H.; Guillou, F.; Zhang, L.; van Dijk, N.H.; Brück, E. Direct measurement of the magnetocaloric effect in MnFe(P, X) (X = As, Ge, Si) materials. *J. Phys. D: Appl. Phys.* **2014**, *47*, 186–187. [CrossRef]
10. Sushmita, D.; Roy, R.K.; Ghosh, M.; Mallick, A.B.; Mitra, A.; Panda, A.K. Enhancement in magnetocaloric properties of NiMnGa alloy through stoichiometric tuned phase transformation and magneto-thermal transitions. *J. Magn. Magn. Mater.* **2017**, *439*, 305–311. [CrossRef]
11. Gao, B.; Hu, F.X.; Shen, J.; Wang, J.; Sun, J.R.; Shen, B.G. Field-induced structural transition and the related magnetic entropy change in $Ni_{43}Mn_{43}Co_3Sn_{11}$ alloy. *J. Magn. Magn. Mater.* **2009**, *321*, 2571–2574. [CrossRef]
12. Zheng, H.X.; Wang, W.; Xue, S.C.; Zhai, Q.J.; Frenzel, J.; Luo, Z.P. Composition-dependent crystal structure and martensitic transformation in Heusler Ni−Mn−Sn alloys. *Acta Mater.* **2013**, *61*, 4648–4656. [CrossRef]
13. Hu, F.X.; Shen, B.G.; Sun, J.R.; Cheng, Z.H.; Rong, G.H.; Zhang, X.X. Influence of negative lattice expansion and metamagnetic transition on magnetic entropy change in the compound $LaFe_{11.4}Si_{1.6}$. *Appl. Phys. Lett.* **2001**, *78*, 3675–3677. [CrossRef]
14. Liu, J.; Krautz, M.; Skokov, K.; Woodcock, T.G.; Gutfleisch, O. Systematic study of the microstructure, entropy change and adiabatic temperature change in optimized La–Fe–Si alloys. *Acta Mater.* **2011**, *59*, 3602–3611. [CrossRef]
15. Hamad, M.A. Tailoring Magnetocaloric Effect in $La_{0.7}Sr_{0.3}MnO_3$–TiO_2. *J. Supercond. Nov. Magn.* **2018**, *31*, 337–340. [CrossRef]
16. Dahal, B.R.; Kyle, S.; Allyn, M.M.; Tackett, R.J.; Huh, Y.; Kharel, P. Near-room-temperature magnetocaloric properties of $La_{1-x}Sr_xMnO_3$ (x = 0.11, 0.17, and 0.19) nanoparticles. *Mater. Res. Express* **2018**, *5*, 106103. [CrossRef]
17. Zehani, K.; Guetari, R.; Mliki, N.; Bessais, L. Study of the Magnetocaloric Effect in $(Pr, Dy)_2Fe_{17}$ and $Pr_2(Fe, Al)_{17}$ Intermetallic Compounds. *Phys. Procedia* **2015**, *75*, 1435–1441. [CrossRef]
18. Dahal, B.; Kharel, P.; Ott, T.; Zhang, W.Y.; Valloppilly, A.; Skomski, R.; Sellmyer, D. Magnetic and magnetocaloric properties of $Pr_{2-x}Nd_xFe_{17}$ ribbons. *AIP Adv.* **2019**, *9*, 035211. [CrossRef]
19. Lyubina, J.; Gutfleisch, O.; Kuz'min, D.M.; Richter, M. $La(Fe,Si)_{13}$-based magnetic refrigerants obtained by novel processing routes. *J. Magn. Magn. Mater.* **2009**, *320*, 2252–2258. [CrossRef]

20. Katter, M.; Zellmann, V.; Reppel, G.W.; Uestuener, K. Magnetocaloric properties of La(Fe,Co,Si)$_{13}$ bulk material prepared by powder metallurgy. *IEEE Trans. Magn.* **2008**, *44*, 3044–3047. [CrossRef]
21. Hansen, B.R.; Kuhn, L.T.; Bahl, C.R.H.; Lundberg, M.; Ancona-Torres, C.; Katter, M. Properties of magnetocaloric La(Fe,Co,Si)$_{13}$ produced by powder metallurgy. *J. Magn. Magn. Mater.* **2010**, *322*, 3447–3454. [CrossRef]
22. Zhong, X.C.; Feng, X.L.; Huang, X.W.; Shen, X.Y.; Liu, Z.W. Structure and magnetocaloric effect of $La_{0.7}Ce_{0.3}(Fe_{0.92}Co_{0.08})_{11.4}Si_{1.6}$ bulk alloy prepared by powder metallurgy. *J. Alloy. Compd.* **2016**, *685*, 913–916. [CrossRef]
23. Bao, L.H.; Wei, W.; Fan, W.D.; Tegus, O. A novel preparation method and magnetic properties of NaZn$_{13}$-type La(Fe,Si)$_{13}$ compounds. *J. Alloy. Compd.* **2014**, *589*, 416–419. [CrossRef]
24. Hou, X.L.; Tian, Y.; Xue, Y.; Liu, C.Y.; Xia, W.X.; Xu, H.; Kelley, P.L.; Srikanth, H.; Phan, M.H. Formation of tree-like and vortex magnetic domains of nanocrystalline α-(Fe,Si) in La−Fe−Si ribbons during rapid solidification and subsequent annealing. *J. Alloy. Compd.* **2016**, *669*, 205–209. [CrossRef]
25. Blazquez, J.S.; Moreno-Ramírez, L.M.; Ipus, J.J.; Kiss, L.F.; Kaptas, D.; Kemeny, T.; Franco, V.; Conde, A. Effect of α-Fe impurities on the field dependence of magnetocaloric response in $LaFe_{11.5}Si_{1.5}$. *J. Alloy. Compd.* **2015**, *646*, 101–105. [CrossRef]
26. Pulko, B.; Tušek, J.; Moore, J.D.; Weise, B.; Skokov, K.; Mityashkin, O.; Kitanovski, A.; Favero, C.; Fajfar, P.; Gutfleisch, O.; et al. Epoxy-bonded La−Fe−Co−Si magnetocaloric plates. *J. Magn. Magn. Mater.* **2015**, *375*, 65–73. [CrossRef]
27. Zhang, H.; Sun, Y.J.; Li, Y.W.; Wu, Y.Y.; Long, Y.; Shen, J.; Hu, F.X.; Sun, J.R.; Shen, B.G. Mechanical properties and magnetocaloric effects in La(Fe,Si)$_{13}$ hydrides bonded with different epoxy resins. *J. Appl. Phys.* **2015**, *117*, 063902. [CrossRef]
28. Zhong, X.C.; Feng, X.L.; Huang, J.H.; Huang, Y.L.; Liu, Z.W.; Ramanujan, R.V. Influence of particle size on the mechanical properties and magnetocaloric effect of $La_{0.8}Ce_{0.2}(Fe_{0.95}Co_{0.05})_{11.8}Si_{1.2}$/Sn composites. *J. Magn. Magn. Mater.* **2018**, *463*, 23–27. [CrossRef]
29. Zhong, X.C.; Feng, X.L.; Huang, J.H.; Jiao, D.L.; Zhang, H.; Qiu, W.Q.; Liu, Z.W.; Ramanujan, R.V. A bimodal particle size distribution enhances mechanical and magnetocaloric properties of low-temperature hot pressed Sn-bonded $La_{0.8}Ce_{0.2}(Fe_{0.95}Co_{0.05})_{11.8}Si_{1.2}$ bulk composites. *J. Magn. Magn. Mater.* **2019**, *469*, 133–137. [CrossRef]
30. Dong, X.T.; Zhong, X.C.; Peng, D.R.; Huang, J.H.; Zhang, H.; Jiao, D.L.; Liu, Z.W.; Ramanujan, R.V. $La_{0.8}Ce_{0.2}(Fe_{0.95}Co_{0.05})_{11.8}Si_{1.2}/Sn_{42}Bi_{58}$ magnetocaloric composites prepared by low temperature hot pressing. *J. Alloy. Compd.* **2018**, *737*, 568–574. [CrossRef]
31. Funk, A.; Freudenberger, J.; Waske, A.; Krautz, M. Getting magnetocaloric materials into good shape: Cold-working of La(Fe,Co,Si)$_{13}$ by powder-in-tube-processing. *Mater. Today Energy* **2018**, *9*, 223. [CrossRef]
32. Wang, Y.X.; Zhang, H.; Liu, E.K.; Zhong, X.C.; Tao, K.; Wu, M.L.; Xing, C.F.; Xiao, Y.N.; Liu, J.; Long, Y. Outstanding comprehensive performance of/In composite with durable service life for magnetic refrigeration. *Adv. Electro. Mater.* **2018**, *4*, 1700636. [CrossRef]
33. Dai, Y.T.; Xu, Z.S.; Luo, Z.P.; Han, K.; Zhai, Q.J.; Zheng, H.X. Phase formation kinetics, hardness and magnetocaloric effect of sub-rapidly solidified $LaFe_{11.6}Si_{1.4}$ plates during isothermal annealing. *J. Magn. Magn. Mater.* **2018**, *454*, 356–361. [CrossRef]
34. Fu, S.; Long, Y.; Sun, Y.Y.; Hu, J. Microstructural evolution and phase transition dependent on annealing temperature and carbon content for $LaFe_{11.5}Si_{1.5}C_x$ compounds prepared by arc-melting. *Intermetallics* **2013**, *39*, 79–83. [CrossRef]
35. Bez, H.N.; Eggert, B.G.F.; Lozano, J.A.; Bahl, C.R.H.; Barbosa, J.R., Jr.; Teixeira, C.S.; Wendhausen, P.A.P. Magnetocaloric effect and H gradient in bulk La(Fe,Si)$_{13}H_y$ magnetic refrigerants obtained by HDSH. *J. Magn. Magn. Mater.* **2015**, *386*, 125–128. [CrossRef]
36. Löwe, K.; Liu, J.; Skokov, K.; Moore, J.D.; Sepehri-Amin, H.; Hono, K.; Katter, M.; Gutfleisch, O. The effect of the thermal decomposition reaction on the mechanical and magnetocaloric properties of La(Fe,Si,Co)$_{13}$. *Acta Mater.* **2012**, *60*, 4268–4276. [CrossRef]
37. Zong, S.T.; Long, Y. The influence of Cr and Ni on the character of magnetic phase transition in $LaFe_{11.52-x}M_xSi_{1.48}$ alloys. *AIP Adv.* **2018**, *8*, 048101. [CrossRef]
38. Md Din, M.F.; Wang, J.L.; Zeng, R.; Shamba, P.; Debnath, J.C.; Dou, S.X. Effects of Cu substitution on structural and magnetic properties of $La_{0.7}Pr_{0.3}Fe_{11.4}Si_{1.6}$ compounds. *Intermetallics* **2013**, *36*, 1–7. [CrossRef]

39. Mican, S.; Tetean, R. Magnetic properties and magnetocaloric effect in $La_{0.7}Nd_{0.3}Fe_{13-x}Si_x$ compounds. *J. Solid State Chem.* **2012**, *187*, 238–243. [CrossRef]
40. Chen, X.; Chen, Y.G.; Tang, Y.B.; Xiao, D.Q. Effect of Ce, Co, B on formation of $LaCo_{13}$-structure phase in $La(Fe,Si)_{13}$ alloys. *Trans. Nonferrous Met. Soc. China* **2014**, *24*, 705–711. [CrossRef]
41. Anh, D.T.K.; Thuy, N.P.; Duc, N.H.; Nhien, T.T.; Nong, N.V. Magnetism and magnetocaloric effect in $La_{1-y}Nd_y(Fe_{0.88}Si_{0.12})_{13}$ compounds. *J. Magn. Magn. Mater.* **2003**, *262*, 427–431. [CrossRef]
42. Rosca, M.; Balli, M.; Fruchart, D.; Gignoux, D.; Hlil, E.K.; Miraglia, S.; Ouladdiaf, B.; Wolfers, P. Neutron diffraction study of $LaFe_{11.31}Si_{1.69}$ and $LaFe_{11.31}Si_{1.69}H_{1.45}$ compounds. *J. Alloy. Compd.* **2010**, *490*, 50–55. [CrossRef]
43. Hai, X.; Mayer, C.; Colin, C.V.; Miraglia, S. In-situ neutron investigation of hydrogen absorption kinetics in $La(Fe_xSi_{1-x})_{13}$ magnetocaloric alloys for room-temperature refrigeration application. *J. Magn. Magn. Mater.* **2016**, *400*, 344–348. [CrossRef]
44. Bao, L.F.; Hu, F.X.; Chen, L.; Wang, J.; Sun, J.R.; Shen, B.G. Magnetocaloric properties of $La(Fe,Si)_{13}$-based material and its hydride prepared by industrial mischmetal. *Appl. Phys. Lett.* **2012**, *101*, 162406. [CrossRef]
45. Shao, Y.Y.; Lu, B.F.; Zhang, M.X.; Liu, J. An X-ray absorption spectroscopy study of La–Fe–Si–(H) magnetocaloric alloys. *Acta Mater.* **2018**, *150*, 206–212. [CrossRef]
46. Liu, J.P.; Fullerton, E.; Gutfleisch, O.; Sellmyer, D.J. *Nanoscale Magnetic Materials and Applications*; Springer: Boston, MA, USA, 2009; ISBN 978-0-387-85600-1.
47. Phejar, M.; Paul-Boncour, V.; Bessais, L. Investigation on structural and magnetocaloric properties of $LaFe_{13-x}Si_x(H,C)_y$ compounds. *J. Solid. State. Chem.* **2016**, *233*, 95–102. [CrossRef]
48. Dai, Y.T.; Li, Y.Q.; Xu, Z.S.; Luo, Z.P.; Han, K.; Zhai, Q.J.; Zheng, H.X. Studying of doping boron and carbon in $LaFe_{11.6}Si_{1.4}$ magnetocaloric alloy by experimental and density-functional methods. *J. Alloy. Compd.* **2018**, *765*, 538–543. [CrossRef]
49. Demuner, A.S.; Takeuchi, A.Y.; Passamani, E.C.; Proveti, J.R.; Larica, C.; Favre-Nicolin, E.; Gomes, A.M. Magnetocaloric properties of the $(La–Gd)Fe_{11.4}Si_{1.6}$ metamagnetic compound. *J. Magn. Magn. Mater.* **2009**, *321*, 1809–1813. [CrossRef]
50. Wu, D.Z.; Xue, S.C.; Frenzel, J.; Eggeler, G.; Zhai, Q.J.; Zheng, H.X. Atomic ordering effect in $Ni_{50}Mn_{37}Sn_{13}$ magnetocaloric ribbons. *Mater. Sci. Eng. A* **2012**, *534*, 568–572. [CrossRef]
51. Li, H.W.; Fang, Y.; Feng, S.T.; Zhai, Q.J.; Luo, Z.P.; Zheng, H.X. Magneto-structural transition behavior in Fe-doped Heusler Mn–Ni–In ribbon materials. *J. Magn. Magn. Mater.* **2016**, *417*, 267–271. [CrossRef]
52. Jia, L.; Sun, J.R.; Shen, J.; Dong, Q.Y.; Hu, F.X.; Zhao, T.Y.; Shen, B.G. Magnetic coupling between rare-earth and iron atoms in the $La_{1-x}R_xFe_{11.5}Si_{1.5}$(R = Ce, Pr, and Nd) intermetallics. *Appl. Phys. Lett.* **2008**, *92*, 182503. [CrossRef]
53. Fujieda, S.; Fujita, A.; Fukamichi, K.; Hirano, N.; Nagaya, S. Large magnetocaloric effects enhanced by partial substitution of Ce for La in $La(Fe_{0.88}Si_{0.12})_{13}$ compound. *J. Alloy. Compd.* **2006**, *408–412*, 1165–1168. [CrossRef]
54. Fujieda, S.; Fujita, A.; Fukamichi, K. Enhancements of magnetocaloric effects in $La(Fe_{0.90}Si_{0.10})_{13}$ and its hydride by partial substitution of Ce for La. *Mater. Trans.* **2004**, *45*, 3228–3231. [CrossRef]
55. Jia, L.; Sun, J.R.; Shen, J.; Dong, Q.Y.; Zou, J.D.; Gao, B.; Zhao, T.Y.; Zhang, H.W.; Hu, F.X.; Shen, B.G. Magnetocaloric effects in the $La(Fe,Si)_{13}$ intermetallics doped by different elements. *J. Appl. Phys.* **2009**, *105*, 07A924. [CrossRef]
56. Balli, M.; Fruchart, D.; Gignoux, D. Optimization of $La(Fe,Co)_{13-x}Si_x$ based compounds for magnetic refrigeration. *J. Phys.: Condens. Matter* **2007**, *19*, 236230. [CrossRef]
57. Wang, F.W.; Kurbakov, A.; Wang, G.J.; Hu, F.X.; Shen, B.G.; Cheng, Z.H. Strong interplay between structure and magnetism in $LaFe_{11.3}Co_{0.6}Si_{1.1}$: A neutron diffraction study. *Phys. B* **2006**, *385–386*, 343–345. [CrossRef]
58. Krautz, M.; Skokov, K.; Gottschall, T.; Teixeira, C.S.; Waske, A.; Liu, J.; Schultz, L.; Gutfleisch, O. Systematic investigation of Mn substituted $La(Fe,Si)_{13}$ alloys and their hydrides for room-temperature magnetocaloric application. *J. Alloy. Compd.* **2014**, *598*, 27–32. [CrossRef]
59. Makarov, S.I.; Krautz, M.; Salamon, S.; Skokov, K.; Teixeira, C.S.; Gutfleisch, O.; Wende, H.; Keune, W. Local electronic and magnetic properties of pure and Mn-containing magnetocaloric $LaFe_{13-x}Si_x$ compounds inferred from Mössbauer spectroscopy and magnetometry. *J. Phys. D Appl. Phys.* **2015**, *48*, 305006. [CrossRef]
60. Bratko, M.; Lovell, E.; Caplin, A.D.; Basso, V.; Barcza, A.; Katter, M.; Cohen, L.F. Determining the first-order character of $La(Fe,Mn,Si)_{13}$. *Phys. Rev. B.* **2017**, *95*, 064411. [CrossRef]

61. Moreno-Ramírez, L.M.; Romero-Muñiz, C.; Law, J.Y.; Franco, V.; Conde, A.; Radulov, I.; Maccari, F.; Skokov, K.P.; Gutfleisch, O. The role of Ni in modifying the order of the phase transition of La(Fe,Ni,Si)$_{13}$. *Acta Mater.* **2018**, *160*, 137–146. [CrossRef]
62. Xu, Z.S.; Dai, Y.T.; Fang, Y.; Luo, Z.P.; Han, K.; Song, C.J.; Zhai, Q.J.; Zheng, H.X. High temperature phase transition behavior and magnetocaloric effect in a sub-rapidly solidified La−Fe−Si plate produced by centrifugal casting. *J. Mater. Sci. Technol.* **2018**, *34*, 1337–1342. [CrossRef]
63. Lai, J.W.; Zheng, Z.G.; Zhong, X.C.; Montemayor, R.; Liu, Z.W.; Zeng, D.C. Magnetocaloric effect of nonstoichiometric $La_{1-x}Fe_{11.4+x}Si_{1.6}$ alloys with first-order and second-order magnetic transitions. *Intermetallics* **2015**, *63*, 7–11. [CrossRef]
64. Chen, X.; Chen, Y.G.; Tang, Y.B. High-temperature phase transition and magnetic property of $LaFe_{11.6}Si_{1.4}$ compound. *J. Alloy. Compd.* **2011**, *509*, 8534–8541. [CrossRef]
65. Chen, X.; Chen, Y.G.; Tang, Y.B. The influence of different cooling processes on phase, microstructure, and magnetocaloric properties of $LaFe_{11.6}Si_{1.4}$ compounds. *Solid State Commun.* **2014**, *186*, 56–63. [CrossRef]
66. Fujieda, S.; Fukamichi, K.; Suzuki, S. Microstructure and isothermal magnetic entropy change of $La(Fe_{0.89}Si_{0.11})_{13}$ in a single-phase formation process by annealing. *J. Alloy. Compd.* **2013**, *566*, 196–200. [CrossRef]
67. Shamba, P.; Zeng, R.; Wang, J.L.; Campbell, S.J.; Dou, S.X. Enhancement of the refrigerant capacity in low level boron doped $La_{0.8}Gd_{0.2}Fe_{11.4}Si_{1.6}$. *J. Magn. Magn. Mater.* **2013**, *331*, 102–108. [CrossRef]
68. Gebara, P.; Pawlik, P.; Hasiak, M. Alteration of negative lattice expansion of the La(Fe,Si)$_{13}$-type phase in $LaFe_{11.14-x}Co_{0.66}Ni_xSi_{1.2}$ alloys. *J. Magn. Magn. Mater.* **2017**, *422*, 61–65. [CrossRef]
69. Zhang, Z.T.; He, C.; Zhang, M.X.; Liu, J. Influence of extra La and annealing temperature on microstructure and magnetocaloric properties of La–Fe–Co–Si alloys. *Phys. B.* **2015**, *476*, 167–170. [CrossRef]
70. Goto, T.; Fukamichi, K.; Yamada, H. Itinerant electron metamagnetism and peculiar magnetic properties observed in *3d* and *5f* intermetallics. *Phys. B* **2001**, *300*, 167–185. [CrossRef]
71. Qian, H.Y.; Dahal, B.; Halbritter, L.; Hu, J.; Huh, Y.; Kharel, P. Structural, magnetic and magnetocaloric properties of $Ni_{43}Mn_{46-x}Fe_xSn_{11}$ (x = 0, 6, 8, 10) alloys. *AIP Adv.* **2019**, *9*, 035005. [CrossRef]
72. Law, J.Y.; Franco, V.; Moreno-Ramírez, L.M.; Conde, A.; Karpenkov, D.Y.; Radulov, L.; Skokov, K.P.; Gutfleisch, O. A quantitative criterion for determining the order of magnetic phase transitions using the magnetocaloric effect. *Nat. Commun.* **2018**, *9*, 2680. [CrossRef]
73. Inoue, J.; Shimizu, M. Volume dependence of the first-order transition temperature for RCo_2 compounds. *J. Phys. F Met. Phys.* **1982**, *12*, 1811. [CrossRef]
74. Segall, M.D.; Lindan, P.J.D.; Probert, M.J.; Pickard, C.J.; Hasnip, P.J.; Clark, S.J.; Payne, M.C. First-principles simulation: ideas, illustrations and the CASTEP code. *J. Phys. Condens. Matter* **2002**, *14*, 2717–2744. [CrossRef]
75. Perdew, J.P.; Chevary, J.A.; Vosko, S.H.; Jackson, K.A.; Pederson, M.R.; Singh, D.J.; Fiolhais, C. Erratum: atoms, molecules, solids, and surfaces: applications of the generalized gradient approximation for exchange and correlation. *Phys. Rev. B* **1993**, *48*, 4978. [CrossRef]
76. Slater, J.C. Atomic Radii in Crystals. *J. Chem. Phys.* **1964**, *41*, 3199–3204. [CrossRef]
77. Greenwood, N.N.; Earnshaw, A. *Chemistry of the Elements*, 2nd ed.; Butterworth-Heinemann: Oxford, UK, 1997; pp. 944–1226. ISBN 978-0-7506-3365-9.